PCCP

Accepted Manuscript

This is an *Accepted Manuscript*, which has been through the Royal Society of Chemistry peer review process and has been accepted for publication.

Accepted Manuscripts are published online shortly after acceptance, before technical editing, formatting and proof reading. Using this free service, authors can make their results available to the community, in citable form, before we publish the edited article. We will replace this *Accepted Manuscript* with the edited and formatted *Advance Article* as soon as it is available.

You can find more information about *Accepted Manuscripts* in the Information for Authors.

Please note that technical editing may introduce minor changes to the text and/or graphics, which may alter content. The journal's standard Terms & Conditions and the Ethical guidelines still apply. In no event shall the Royal Society of Chemistry be held responsible for any errors or omissions in this *Accepted Manuscript* or any consequences arising from the use of any information it contains.

ROYAL SOCIETY OF CHEMISTRY

www.rsc.org/pccp

Trends in the Adsorption and Reactivity of Hydrogen on Magnesium Silicate Nanoclusters

Ichraf Oueslati[a,b], Boutheïna Kerkeni[a,c], Stefan T. Bromley*[d,e]

[a] *Faculté des Sciences de Tunis, Département de Physique, (LPMC), Université de Tunis El Manar, 2092 Tunis, Tunisia*

[b] *LERMA, UMR8112-CNRS, Observatoire de Paris, Université Pierre et Marie Curie, 5 place Jules Janssen, 92195 Meudon Cedex, France*

[c] *Institut Supérieur des Arts Multimédia de la Manouba, Université de la Manouba, 2010 la Manouba, Tunisia*

[d] *Department de Química Física & Institut de Química Teòrica i Computacional, Universitat de Barcelona, C/ Martí i Franquès 1, E-08028 Barcelona, Spain*

[e] *Institució Catalana de Recerca i Estudis Avançats (ICREA), E-08010 Barcelona, Spain.*

**Corresponding author; E-mail: s.bromley@ub.edu*

Abstract

We study nanoclusters of Mg-rich olivine and pyroxene (having $(MgO)_6(SiO_2)_3$ and $(MgO)_4(SiO_2)_4$ compositions) with respect to their reactivity towards hydrogen atoms, using density functional calculations. Ultrasmall silicate particles are fundamental intermediates in cosmic dust grain formation and processing, and are thought to make up a significant mass fraction of the grain population. Due to their nanoscale dimensions and high surface area to bulk ratios, they are likely to also have a disproportionately large influence on surface chemistry in the interstellar medium. This work investigates the potential role of silicate nanoclusters in vital interstellar hydrogen-based chemistry by studying atomic H adsorption and H_2 formation. Our extensive set of calculations confirm the generality of a Brønsted–Evans–Polanyi (BEP) relation between the H_2 reaction barrier and the $2H_{chem}$ binding energy, suggesting it to be independent of silicate dust grain shape, size, crystallinity and composition. Our results also suggest that amorphous/porous grains with forsteritic composition would tend to dissociate H_2, but relatively Mg-poor silicate grains (e.g. enstatite composition) and/or more crystalline/compact silicate grains would tend to catalyse H_2 formation. The high structural thermostability of silicate nanoclusters with respect to the heat released during exothermic H_2 formation reactions is also verified.

Introduction

H_2 is the most abundant molecule in the universe and is crucially involved in the formation of more complex molecular species in the interstellar medium (ISM), e.g. the chemistry in interstellar clouds[1]. Due to its chemical importance, there is much interest in understanding the mechanisms and formation rates of this vital H_2 feedstock, which needs to be continuously generated from ubiquitous hydrogen atoms. It is widely accepted that the H_2 production reaction most likely occurs on dust grains,[2,3,4] as all competing gas phase processes are much less efficient at the low interstellar temperatures and gas pressures. The adsorption of atomic hydrogen on small dust particles, can open up reaction pathways which allow for H_2 formation to proceed with relatively reduced barriers. The H_2 formation reaction is also highly exothermic (-434 kJ/mol) with heat that must be dissipated to avoid dissociation of the product. Although significant amounts of energy can go into the internal energy and translational kinetic energy of the formed H_2 molecule,[5,6,7,8] dust particles can also play the role of a third body to dissipate a significant percentage of the energy released leading to more stable H_2 molecules.

Most interstellar dust is thought to be formed in the stellar winds of large dying stars[9,10] and has a chemical composition that depends on that of the parent star. Two main families of dust types are thus formed in circumstellar environments: (i) carbonaceous and silicon carbide grains in carbon-rich atmospheres, and (ii) magnesium rich silicate grains in the atmospheres of oxygen-rich stars.[11] After formation the stardust is ejected into the ISM where it is subjected to a multitude of processes (e.g. amorphized by high energy radiation and shockwaves) and eventually incorporated into the relative shelter of interstellar clouds where chemistry can more readily occur.[12] Of the two main families of dust, we focus on silicate grains which are the most abundant and least well understood family of solids in space.[11] Specifically, our study concentrates on nanosilicates and their chemical interactions with hydrogen. These nanosilicates are fundamental intermediates in silicate dust formation in stellar outflows, are likely to result from processing of large silicate grains, and are ubiquitous throughout the ISM. Specifically, it has been estimated that 10% of the mass fraction of the interstellar silicate grain population is made up of nanoclusters with ≤1.5 Å diameters.[13] By studying such small species we aim to probe the lower size limit of silicate dust grains with respect to their cosmic chemical importance.

The properties of ultra small silicate nanoclusters are extremely difficult to examine in detail through experimental laboratory or observational means, and experimental studies have focussed on bulk silicate surfaces. In particular, H_2 formation has been experimentally studied on surface of polycrystalline[14] and amorphous silicates.[15,16,17] Quantum chemistry based computational modelling can help to augment our understanding of these systems by providing uniquely detailed insights into many properties of silicates, such as: atomic and electronic structures, thermodynamic stabilities,

vibrational spectra, absorption spectra, formation pathways, and chemical reactivity.[18] Previously, via such a computational chemistry approach, the thermodynamic properties of many step-wise additive cluster intermediates based predominately on the abundant Mg, SiO, H_2O species were determined[19,20], providing an unprecedented level of detail into nucleation pathways relevant to silicate dust formation in various astronomical environments. Chemical reactivities of silicate nanoclusters towards H_2 and H_2O have also been studied by computational quantum chemical modelling.[12,21] Addressing the issue of oxygen depletion in dense interstellar clouds it was found that a stable nanopyroxene cluster with a $(MgO)_4(SiO_2)_4$ composition, could act as an oxygen sink by being significantly overoxidized by water molecules via the formation of surface hydroxyl groups.[12] With respect to the subject of the present work, for one nanosilicate cluster isomer having the $(MgO)_6(SiO_2)_3$ composition, calculations have also confirmed that nanosilicates could offer several routes to H_2 formation and dissociation.[21] Similar calculations have also examined H_2 formation on the regular (010) surface of forsterite (i.e. the crystalline bulk silicate with $SiO_2(MgO)_2$ stoichiometry) using an embedded cluster approach[22] and periodic models.[8,23,24] We note that the majority of silicate dust grains in the ISM are amorphous and modelling using regular crystalline surfaces may not be the most structurally appropriate approach for such systems. On the other hand the nanosilicates that we study herein are so small as to be inherently non-crystalline and can thus be also regarded as a way to simulate the effects of amorphicity within a small model system.

In a previous study[21], using the most energetically stable $(MgO)_6(SiO_2)_3$ cluster isomer structure, we considered a single mechanism for H_2 formation and dissociation which involved two types of chemisorbed H atoms: (i) $O\text{-}H^+_{chem}$ protonation of an oxygen anion site, together with (ii) H^-_{chem} forming a Mg-H hydride bond. These two sites were found to be associated with one another as the prior formation of $O\text{-}H^+_{chem}$ would entail transfer of negative charge from the oxygen site to a nearby Mg cation site, where formation of the second H^-_{chem} would be facilitated (i.e. $[H^+_{chem} \rightarrow H^-_{chem}]$ sequential chemisorption of two separate H atoms, $2H_{chem}$). For this cluster and this formation/dissociation mechanism for H_2 we also showed that a Brønsted–Evans–Polanyi (BEP) relation (i.e. where the activation energies of a set of reactions of the same family are proportional to their enthalpies of reaction) existed between the transition state energy of H_2 formation and the $[H^+_{chem} \rightarrow H^-_{chem}]$ adsorption energy of the two H atoms.

The aim of the present study is first to establish whether the above behaviour is not only general to the most stable olivine $(MgO)_6(SiO_2)_3$ cluster isomer (i.e. nano-olivine_c in Fig. 1c), but to other structural isomers of olivine clusters of the same size and composition, and to similar sized nanosilicate clusters of different stoichiometry. For all considered nanoclusters (see Fig. 1) we have calculated the energetic pathways associated with: H adsorption, diffusion, recombination and H_2 molecular desorption. With our new results we confirm the generality of the H_2 reaction barrier *versus* $2H_{chem}$ binding energy BEP relation for silicates with 20 data points (including six data points from

our previous study[21] and a data point from a bulk forsterite surface theoretical study[22]). We find that the strength of the [$H^+_{chem} \rightarrow H^-_{chem}$] type adsorption process is linked to the distance between the adsorbed polarised H atoms. We further find new highly strongly bound $2H_{chem}$ adsorption configurations on some silicate clusters that can be interpreted as being of a new [$H^-_{chem} \rightarrow H^+_{chem}$] type rather than the [$H^+_{chem} \rightarrow H^-_{chem}$] as has been previously reported.[8,21] Corresponding data points from this latter type of adsorption are also found to follow the general BEP relation. In all cases the $2H_{chem}$ binding energy is also found to be proportional to the binding energy of only the H^+_{chem} species. Comparison with the BEP relation implies that the latter energetic contribution is correlated to the height of the H_2 reaction barrier. Further analysis of this latter trend, suggests that although the [$H^+_{chem.} \rightarrow H^-_{chem}$] type of adsorption will be more prevalent for lower total binding energies of both H atoms, the [$H^-_{chem} \rightarrow H^+_{chem}$] type of adsorption process will be more common for larger $2H_{chem}$ binding energies. This in turn suggests that the former type of adsorption will tend to lead to H_2 formation, and the latter mode to H_2 dissociation. From further considering which types of magnesium silicates tend to promote for which types of $2H_{chem}$ adsorption modes, we further speculate on how structure (e.g. amorphous, porous, crystalline) and Mg-content could be related to the propensity of silicate grains to form H_2.

Finally, due to the very small size of the nanosilicate clusters we consider, it is conceivable that highly exothermic reactions could significantly perturb, or even destroy, their structural integrity thus potentially changing, or even removing their influence, on subsequent chemical reactions. In order to check this possibility, we explicitly consider the thermodynamic stability of two of our nanosilicate clusters at a temperature estimated to be typically induced through the energy release of the H_2 formation reaction.

Methodology

We consider a number of Mg-rich olivine and pyroxene nanocluster isomers with compositions $(MgO)_6(SiO_2)_3$ and $(MgO)_4(SiO_2)_4$ (i.e. having $(MgO)_{2n}(SiO_2)_n$ forsterite and $(MgO)_n(SiO_2)_n$ enstatite stoichiometies, respectively), as shown in Fig. 1. We label these clusters as: nano-olivine_a (Fig. 1a), nano-olivine_b (Fig. 1b) and nano-pyroxene (Fig. 1d). For reference with our previous study,[21] we also label the lowest energy $(MgO)_6(SiO_2)$ cluster isomer as nano-olivine_c (Fig. 1c). All these nanosilicate clusters were found through global optimization using the methodology detailed in previous works.[12,19] Due to their very small size all considered clusters do not yet exhibit bulk crystallinity, but all have complete SiO_4 tetrahedra which are either directly joined together through a bridging oxygen (Si-O-Si) linkage, or separated by Mg cations.

For structural optimisations, and for computing harmonic frequencies and transition states, density functional theory (DFT) calculations have been performed using the Gaussian 09 program.[25]

The MPWB1K hybrid meta-functional was employed since it has been proven useful to study both systems with weak interactions as well as providing accurate activation barrier energies.[21,22,26,27,28] This functional has also been employed in previous studies of hydrogenation processes in the interstellar medium[12,21,22], thus allowing for comparison with previous data. For Mg and Si atoms, we used a 6-31G(d) basis set and for O and H atoms we used a 6-31+G(d,p) set of basis functions. In all optimisations, all atom positions in the cluster together with any reactants/products were fully relaxed with no symmetry constraints. The structures resulting from the optimisations were checked to have all positive frequencies and thus be true local energy minima. Transition states were obtained using the synchronous transit-guided quasi-Newton method[29] and were all verified to have a single imaginary vibrational frequency along the reaction coordinate (see Supplementary Information for lists of all vibrational frequencies). Using this methodology, the nano-olivine_a and nano-olivine_b nanoclusters are found to be metastable with respect to the ground state nanocluster of this composition (i.e nano-olivine_c) by 39 kJ/mol and 51 kJ/mol, per $(MgO)_2(SiO_2)$ formula unit, respectively. The nano-pyroxene cluster studied is the ground state $(MgO)_4(SiO_2)_4$ nanocluster isomer.

The binding energy of a *n* separated H atoms with a nanocluster is defined as: E_{bind} = -[E(cluster + *n*.H) - E(*n*.H) - E(cluster)], where E(cluster + *n*.H) is the energy of *n* H atoms adsorbed on the cluster, E(H) is the energy of the free H atom and E(cluster) is the energy of the cluster. E_{bind} values and other energies are given in kJ/mol and rounded to the nearest kJ/mol to reflect the typical accuracy of DFT methods. When comparing with previous work where Kelvin has been used as an energy unit, the non-rounded kJ/mol value is converted to Kelvin. We note that we report E_{bind} values that are uncorrected for basis set superposition error (BSSE) so that we can compare our results directly with similar data from previous studies. One previous study has indicated that BSSE is most significant for hydrogen physisorption, where it has been shown that it can lead to overestimates of E_{bind} values by between 10-41%, depending on the physisorption type and basis set employed.[8] Our calculations of BSSE effects for four different physisorption configurations on two clusters (see Supplementary Information) also concur that the uncorrected E_{bind} values are similarly between 18-45% too large. The majority of our results, however, concern chemisorbed H atom configurations where BSSE effects typically lead to systematically smaller average E_{bind} overestimates. For DFT calculations of H chemisorption on the forsterite surface using a moderately large basis set, BSSE was found to account for 8% of E_{bind}.[8] In the present study, considering nine chemisorption configurations on two nanoclusters (see Supplementary Information), we find on average that BSSE accounts for ~5% of our reported E_{bind} values. As this effect is relatively small, and, moreover, that we are more concerned with trends in reactivity and E_{bind} values (which would not be affected by such effects), we do not apply this correction to our reported chemisorption values.

Canonical *ab initio* molecular dynamics (AIMD) calculations of 28 picoseconds (3 ps of equilibration followed by 25 ps production) at a temperature of 800 K were performed on the nano-

olivine_c and the nano-pyroxene clusters employing a 0.5 femtosecond time step and the Bussi-Donadio-Parinello thermostat[30]. The energies and forces during the AIMD runs were calculated using DFT employing the PBE functional[31] and a light basis as implemented in the FHI-AIMS code[32].

Results and Discussion

Physisorption of H atoms

The nano-olivine_a and nano-pyroxene clusters offer a variety of sites for impinging gas phase hydrogen atoms. Three physisorption sites for H atoms were found: (i) P1, atop an Mg cation, (ii) P2, above an Mg-O bond, and (iii) P3, over the centre of rings circumscribed by the atoms MgOSiOMgO or OSiOMgOSiO. We remind that reader BSSE is likely to account for ~3-6 kJ/mol of both our reported E_{bind} values, and the E_{bind} values from the literature that we compare our data with.

For the nano-pyroxene cluster, only P2 sites were found. Fig. 2a and Fig. 2.b show the physisorption of a H atom with distances of 2.06 Å and 1.94 Å from a Mg cation and 1.93 Å and 1.80 Å from an O anion, respectively. These configurations have quite strong binding energies of 11 kJ/mol and 19 kJ/mol, respectively.

For the the nano-olivine_a cluster, H atoms can adsorb on P1, P2 and P3 sites. The P2 sites are shown in Fig. 2c and Fig. 2d. Here the H atom is physisorbed over an Mg–O bond with distances of 2.06 Å and 2.03 Å from the Mg cation and 1.94 Å and 1.87 Å from the O anion, respectively. The corresponding E_{bind} values are 9 kJ/mol [1045 K] and 16 kJ/mol [1876 K]. For a similar P2 adsorption site on the nano-olivine_c cluster, a binding energy of 11 kJ/mol [1327 K] was previously reported,[21] while for the crystalline forsterite (010) surface, P2 physisorption binding energies have been calculated to be between 10 kJ/mol[22] and 17 kJ/mol.[8]

Fig. 2e corresponds to the physisorption of H atom on P1 site of the nano-olivine_a cluster at a distance of 2.47 Å from a Mg cation. This configuration has a fairly low E_{bind} value of 7 kJ/mol [864 K] and is very similar in magnitude to that reported for the nano-olivine_c cluster (788 K)[21]. For the forsterite (010) surface, Navarro-Ruiz et al.[8] found that a H atom can physisorb fairly strongly (14 kJ/mol) on top of a Mg cation which is surrounded by three oxygen surface anions. In this case the anions are thought to attract the incoming gaseous H atom and then contribute to increase the non-bonded electrostatic interaction.[8]

The strongest physisorption was found for a P3 site on the nano-olivine_a cluster whereby a H atom lays above the centre of an MgOSiOMgO ring, as shown in Fig. 2f with the strongest binding energy (17 kJ/mol). Another P3 site (OSiOMgOSiO ring) was also found with the weakest binding energy (5 kJ/mol) of all (not shown). For this weakly bound configuration, the smallest O-H and Mg-H distances were found to be 2.40 Å and 2.65 Å respectively.

The present results can be compared with experimental data reported by Katz et al.[33] and Perets et al.[15]. In the latter the energy barriers for atomic H desorption were obtained by fitting temperature programmed desorption curves for polycrystalline[33] and amorphous[15] silicate surfaces. The smallest physisorption binding energy of a single H atom on nano-olivine_a (5 kJ/mol [644K]) is close to the experimental values of 4 kJ/mol [513 K][15] and 3 kJ/mol [373 K][33]. Generally speaking, however, the calculated physisorption E_{bind} values are higher than that found in experiment. We note that the generally higher values reported above are likely to be overestimates due to BSSE effects which may go some way to help to explain the disagreement. The difference between experimental and theory may also be due to the fact that experimental surface is likely to be partially hydroxylated[34] which would shield the direct interaction with surface ions and thus attract H atoms less strongly.

The transition energies between physisorbed states were calculated in order to study the diffusion behaviour of hydrogen atoms on the nano-olivine_a cluster. The barrier for atomic hydrogen to jump between the configuration which has the highest physisorption binding energy (P3 site in 2f), and the configuration (P1 site in 2e) that has the lowest, is about 15 kJ/mol [1753 K]. The calculated activation energy is less than that found in ref [21] (2398 K) for the analogous H diffusion case, which can be explained by the relatively high strength of the P3 binding energy of physisorbed H atom on the MgOSiOMgO ring (2894 K) in this study. For all presently studied sites, H atoms can diffuse over the surface of the clusters with activation barriers ranging between <1 kJ/mol and 15 kJ/mol. All physisorption binding energies are summarised in Table 1.

Chemisorption of H atoms

Chemisorption of a single H atom can occur at two different types of site: (i) C1-type, by attachment of H^{+}_{chem} to an O anion, and (ii) C2-type, by bonding of H^{-}_{chem} to a MgOMgO ring. On all C1 sites of the nano-pyroxene cluster and the majority of those on the nano-olivine_a cluster, the H atom chemisorbs to an oxygen anion that is bonded to a Si cation. Due to the resulting negative charge transfer to a nearby Mg cation, this type of chemisorption leads to structural rearrangement (stretching/breaking of a nearby Mg-O bond). H^{+}_{chem} species at this type of C1 chemisorption site on the nano-pyroxene cluster have binding energies between 69-200 kJ/mol [8262-24106 K] (see Fig. 3). These results are in line with previous calculations using a slightly different DFT set-up which reported that a H atoms can chemisorb on the nanopyroxene cluster with a range between 9284 and 23000 K[12]. The hydrogen adsorption process on a C1 site of the nano-olivine_a cluster gives a range of binding energies between 43-272 kJ/mol [5120-32698 K] which lay above and below those calculated for the nano-olivine_c cluster[21] (adsorption energy range between 9115 and 22640 K) and for the foresterite (010) surface (68[8], 101[22] and 78[24] kJ/mol). The strongest C1-type binding energies of $H^{+}_{chem.}$, however, were found for configurations corresponding to Fig. 4g in this work and to Fig. 3f

in ref [21]. In both these configurations, a MgOHMg group is formed instead of a SiOH group and no Mg-O bond is broken.

We performed a Mulliken atomic charge population analysis before and after chemisorption for all C1 configurations in order to identify the Mg cation that receives the negative charge (labelled in Fig. 3 and Fig. 4 by black arrows). We note that although Mulliken partitioned atomic charges are not particularly accurate when considering how they reproduce observables such as molecular dipole moments, as long as a consistent basis set is used throughout, such charges are known to be sufficient to capture trends with respect to changes in the extent of charge transfer. For those C1 configurations corresponding to Figs. 3c-d and 3g (i.e on the nano-pyroxene cluster) and Figs. 4b, 4d-e, 4g (i.e. on the nano-olivine_a cluster) and 4h (i.e. on the nano-olivine_b cluster), the negative charge localization occurs at the Mg cation bonded to the pre-protonated oxygen anion, resulting in a reduction in the Mg cation positive charge by between +0.34e and +0.45e. Note that the cluster structures in Figs 3 and 4 show the optimised final C1 states in which the Mg-O bond has often been broken upon charge transfer. For the remaining C1 configurations, the donation of negative charge from the O anion after the chemisorption of the H atom, is made to a Mg cation that is not the one bonded to the pre-protonated O atom but is located on the periphery of the nanocluster and linked to two O atoms. In these cases a relatively larger decrease in the Mg positive charge is found (between +0.48e and +0.58e) as measured by differences in Mulliken partitioned charges.

The conversion of physisorbed H atoms to chemisorbed H atoms was considered through studying the transition from P3 sites to C1 sites on the nano-olivine_a cluster. The largest activation energy barrier for physisorption-to-chemisorption was found to be 8 kJ/mol (1013 K). This corresponds to the transfer of an H atom from the P3 configuration having the strongest physisorption binding energy (Fig. 2f), to the C1 site depicted in Fig. 4d and is slightly higher than that found previously on the nano-olivine_c cluster (855 K).[21] The transition process from sites of type P2 to sites of type C1 has been the subject of previous studies of H_2 formation on the (010) surface of foresterite.[22,8] where the reported activation barriers (10-27 kJ/mol) are greater than we find (4 kJ/mol).

In all our considered cases as the released energy due to physisorption is greater than the activation energy, the barrier to chemisorption can be easily overcome. Therefore, we conclude that hydrogen chemisorption at C1 sites via physisorbed sites on the nano-olivine_a cluster is effectively barrierless. For configurations corresponding to Figs. 4a, 4c, 4f and 4g, impinging gas-phase H atoms can directly chemisorb in a barrierless manner. Conversely, Downing *et al*[24] found a barrier of 14 kJ/mol for direct chemisorption of a H atom on a C1 site on the (010) forsterite surface. Although this latter study and the present work use different DFT calculation set-ups, the presence or not of a barrier is likely due to the significant difference in structure between the small amorphous-like olivine_a cluster and the extended crystalline silicate surface.

H atoms can also directly adsorb at C2 sites on the nano-olivine_a cluster without any barrier above the centre of a MgOMgO ring (see Fig. 5d) and a MgOMgOMgO ring (see Fig. 5e). The binding energies of an H atom at these two sites are 91 kJ/mol and 105 kJ/mol, respectively, which are in a comparable range to those found for the C1 site (see Table. 2). The $(MgO)_n$ rings appear to trap the H atoms as H^-_{chem} species through strong interactions with at least two Mg atoms, which synergistically attract it. H at the smaller ring C2 site has Mg-H bonds of 1.874 and 2.092 Å, while at the larger ring C2 site the two smallest Mg-H distances are 1.844 Å, 1.951 Å, with one larger distance of 3.18 Å. The analysis of Mulliken atomic partitioned charges shows that the adsorbed H atom is negatively charged (-0.18e and -0.11e for the configurations shown in Figs. 5d and 5e respectively) which confirms that a hydride like Mg-H bond is formed. Downing et al.[24] predicted that H atoms could chemisorb above single Mg cation on the foresterite surface (010) with adsorption energy of 43 kJ/mol. The fact that this value is significantly lower than that found in this work is probably due to the relative inaccessibility of Mg cations on the (010) forsterite surface where, at most, one Mg cation is available for any one H atom. Conversely, on silicate nanoclusters, where most of the atoms are at the surface, and which structurally do not have the regular dense crystalline packing of forsterite, it is easier to find more than one accessible Mg cation site in close proximity. This rational would also tend to favour C2 sites occurring more frequently on more Mg-rich silicate nanoclusters (i.e. higher Mg:Si ratios) as is confirmed by our results where C2 sites are only found on the 2:1 $(MgO)_6(SiO_2)_3$ nano-olivine_a cluster and not on the 1:1 $(MgO)_4(SiO_2)_4$ nano-pyroxene cluster.

As only two examples of a C2 site were found on the nano-olivine_a cluster, we examined other possible clusters for this site. Firstly, on the nano-olivine_b cluster (see Fig. 1b) we found that a H atom can be adsorbed close to a MgOMgOSiO ring where it lays most closely to two Mg atoms with Mg-H distances of 2.01 and 2.06 Å (see Fig. 5c). The H atom at this site has a E_{bind} value of 38 kJ/mol and the analysis of Mulliken atomic charge on the Mg sites confirms the formation of hydride Mg-H bonding. We thus conclude that this is another example of a C2 site. For the nano-olivine_c cluster, the only configuration with a chemisorbed hydrid-like H^-_{chem} species we could find is illustrated in Fig. 5a. Clearly this H adsorption configuration produces a structural rearrangement (i.e. a broken Mg-O bond) compared to the relaxed structure in Fig. 1c. Our calculations show that the formation of such a C2 site requires energy, resulting in a negative E_{bind} value of -74 kJ/mol with respect to the original relaxed bare cluster. Going to the extreme case of Mg-rich clusters which exhibit no Si atoms, we also attempted to find C2 H^-_{chem} binding sites on the ground state $(MgO)_6$ cluster. We found that H atoms can chemisorb at a C2 site (see Fig. 5b) but, as in the nano-olivine_c case, this reaction is endothermic (E_{bind} of -25 kJ/mol) since it needs energy to break a Mg-O bond.

In both the above cases where the C2 chemisorption is endothermic, the original cluster is the most stable one known for its composition and is thus tend to be structurally compact. Conversely, for the two cases where exothermic C2 adsorption is found, the clusters are slightly metastable with respect to the respective ground state cluster isomer and have accordingly more open structures.

Overall, based on these preliminary data, we tentatively suggest that C2-type adsorption could be most energetically favoured on moderately Mg-rich silicate dust grains (e.g. forsteritic composition) with non-compact (e.g. porous and/or amorphous rather than crystalline) surfaces.

Adsorption of a second H atom

A second gas phase H atom can adsorb on our nanosilicate clusters without a barrier. The binding energies of the second H atom are all considerably larger than that of the first chemisorbed H atom (see Table 2). In all cases of clusters possessing a H atom chemisorbed at a C1 (i.e. $H^{+}_{chem.}$) site, the transfer of negative charge to a single Mg cation results in a subsequent H atom forming a Mg^{+}-H^{-} (C3) hydride species (see Fig. 6 and Fig. 7 for nanopyroxene and nano-olivine_a clusters, respectively) at the Mg site to which the charge is transferred. The charge transfer to a Mg cation due to the formation of a C1 site, and the subsequent energetically favourable adsorption of H in a C3 manner at this electron-accepting Mg site has been confirmed in other studies.[8,21,22] This C1/C3 $2H_{chem}$ adsorption mode is stabilized by favorable electrostatic interactions between the $H^{+}_{chem.}$+H^{-}_{chem} surface species. Using our relatively large data set, in Fig. 8, we plot the binding energy of the second H^{-}_{chem} atom to the respective cluster with one H^{+}_{chem} atom already adsorbed at a C1 site, versus the distance between the two adsorbed H atoms. Our results reveal two trends for C1/C3 $2H_{chem}$ adsorption. Firstly, for H-H distances less than approximately 4.8 Å, the binding energy of the second atom is inversely proportional to the H-H bond distance (i.e. the smaller the distance, the greater the adsorption energy of the second H). In this range of H-H separations the electrostatic interaction stabilises the C1/C3 pair, but more weakly with increasing H-H separation (see blue shaded area in Fig. 8). However, when the H-H distance is larger than ~4.8 Å, the binding energies of the second H atom are relatively stable (see red shaded area in Fig. 8). For these larger H-H separations the electrostatic interaction does not appear to play an important role in energetic stabilization.

When the first H atom is chemisorbed on a C2 site, this causes a negative charge decrease on a nearby O atom which then becomes the most energetically favourable site for an incoming gas-phase H atom for protonation. The chemisorption of the second H in this case increases the negative charge on the charge-depleted oxygen centre by between 0.45-0.52e. We note that these configurations (see Figs. 9a-d) have the most strongly bound second H atoms (see Table 2). For 9a and 9b (nano-olivine_a) the second H atoms adsorb in a C1 manner at a site which is very similar to that shown in Fig. 4g, which is the site with the highest E_{bind} value for a single H atom. Similarly, the second C1 adsorbed H atom in configuration 9c (nano-olivine_b) is almost exactly the same as that found in Fig. 4h, which is the H-adsorbed configuration with the second highest E_{bind} value. For these three cases this C2 → C1 (i.e [H^{-}_{chem}→ H^{+}_{chem}].) adsorption process is also found to lead to the most strongly bound pair of H atoms. In the case of configuration 9d on nano-olivine_c, although the second C1-type H chemisorption has a relatively high E_{bind} value, the first C2-type absorption is endothermic due

to the disruption of the structure of the cluster (Fig. 5a). Thus, in this case the final binding energy of two H atoms is relatively moderated. We note that, although there are several C1 sites that are energetically more favourable for adsorption of a single H atom than the C2 sites discovered herein. However, C1-type H adsorption (e.g. configuration 4g) tends to favour only one Mg atom for subsequent H adsorption (e.g. 4g → 7d). Overal such C1→ C3 processes yield more weakly bound $2H_{chem}$ configurations than the $2H_{chem}$ configurations found to be naturally favoured from C2 → C1 adsorption (e.g. 9a-c).

Formation of H_2

Two chemisorbed H atoms can recombine via a transition state and yield a physisorbed H_2 molecule ($H_{2,phys}$) that can subsequently desorb to form H_2 in gas phase ($H_{2,g}$). Several reactions paths were found on the nano-pyroxene and nano-olivine_a clusters. In Table 3, the ($2H_{chem} \rightarrow H_{2,phys}$) reaction energy, the transition state energy corresponding to the TS[$2H_{chem} \rightarrow H_{2,phys}$] reaction barrier, and the $H_{2,phys} \rightarrow H_{2,g}$ desorption energy were calculated for reaction paths starting from the configurations of two chemisorbed H atoms shown in Fig. 6, Fig. 7 and Fig. 9. Only for configurations corresponding to Fig. 6c, Fig. 6g and Fig. 7a, and were we unable to locate a TS[$2H_{chem} \rightarrow H_{2,phys}$] transition state.

The most energetically favourable channels for $H_{2,phys}$ formation correspond to reactions starting from $2H_{chem}$ configurations shown in Figs. 6d-f for the nano-pyroxene cluster, those shown in Figs. 7a-b, 7f and 7g for the nano-olivine_a cluster. These configurations generally lead to exothermic $H_{2,g}$ formation, except for those in Figs. 6f and 7f, where the energy required for the desorption of the $H_{2,phys}$ is higher than the energy released from two chemisorbed H atoms to form physisorbed H_2. The remaining configurations are precursor states to endothermic H_2 formation (see Table. 3).

In Fig. 10, we plot the most exothermic and endothermic energy profiles leading to $H_{2,g}$ formation starting from configurations shown in Fig. 6, Fig. 7 and Fig. 9. Following ref 21 we take the sum of the energies of the bare relaxed nano-olivine_c cluster and a $H_{2,g}$ molecule as a common zero energy. For the nano-pyroxene cluster, reaction paths from configurations 6d and 6e have the highest exothermicities of -94 kJ/mol and -71 kJ/mol, the lowest activation energies of 8 kJ/mol and 45 kJ/mol, and the smallest $2H_{chem}$ binding energies of 380 kJ/mol and 403 kJ/mol, each respectively. For the nano-olivine_a cluster, the most energetically favourable reaction paths to form $H_{2,g}$ start from configurations 7a and 7g. These two paths have the lowest total $2H_{chem}$ binding energies of 352 kJ/mol and 426 kJ/mol, respectively, and the highest exothermicities of -123 kJ/mol and -44 kJ/mol, respectively. Configuration 7g also leads to the lowest calculated barrier (22 kJ/mol) of all reaction paths considered. As noted above, a transition state could not be located for reactions starting from configuration 7a, which leads to the most efficient catalytic path for $H_{2,g}$ formation. $H_{2,g}$ formation is generally more favoured on the nano-olivine_a cluster compared with the nano-olivine_c cluster, the nano-pyroxene cluster and the foresterite surface.[22] For all nanosilicate clusters studied, we have

found at least one H_2 formation route that is more energetically favourable than that of the corresponding bulk surface reaction pathway.[22]

The remaining reaction paths discovered on the clusters are endothermic and they therefore inhibit $H_{2,g}$ formation. They have the strongest total binding energy of two chemisorbed H atoms and, correspondingly, also have a large activation energy (see Table. 3) required to break the Mg^+-H^- bond and to react with a chemisorbed H^+_{chem}. We plot also in Fig. 10 the most and the least reactive profiles relative to $H_{2,g}$ formation on nano-olivine_c (we refer the reader to Fig. 5 in ref [21]). We found that the nano-olivine_a has more sites to catalyse the dissociation of $H_{2,g}$ than the nano-olivine_c.

In previous work considering a few reaction paths on the nano-olivine_c cluster,[21] it was suggested that the H_2 dissociation reaction followed a BEP relation. In order to confirm whether this BEP relation is more general to other bare silicate grains with different structures and compositions, in Fig. 11 we plot the energy of the TS[$2H_{chem} \rightarrow H_{2,phys}$] transition state barrier height as function of the $2H_{chem}$ binding energy atoms for all calculated reaction paths. Data from Kerkeni and Bromley[21] corresponding to the nano-olivine_c cluster and from Goumans et al.[22] corresponding to foresterite surface (010) are also plotted. The results show that all data points follow the same trend whereby the barrier height is linearly dependent on the total $2H_{chem}$ binding energy, clearly extending the BEP relation to all new reactions and clusters studied in the present work. This result is particularly significant as the present work includes: (i) non-olivinic type clusters (e.g. nano-pyroxene), (ii) clusters which are metastable with respect to the ground state cluster isomers for their composition (e.g. nano-olivine_a and nano-olivine_b), and (iii) clusters with particularly strongly chemisorbed H atoms that can be interpreted as being formed through a novel [$H^-_{chem} \rightarrow H^+_{chem.}$] (i.e. C2 → C1) type of adsorption process. Taken together, all data in Fig. 11 thus provide more evidence to support the claim that H_2 dissociation on bare magnesium silicates follows a general BEP relation independently of silicate dust grain, shape, size, crystallinity and composition.

Of all the reaction energy profiles studied, those corresponding to configurations 7d, 9a and 9b are the most energetically favourable for the dissociation of molecular hydrogen. The differences in the exothermicity of these pathways with respect to H_2 dissociation appear to be linked to relatively high $2H_{chem}$ binding energies. Although configuration 7d, exhibits a C1/C3 type of $2H_{chem}$ adsorption, the reaction paths corresponding to configurations 9a and 9b start from C2/C1 H_{chem} adsorption. This observation suggests that reaction paths starting by H adsorption on Mg-O rich areas (C2 sites) on silicate dust grains may be more likely to inhibit $H_{2,g}$ formation. To further investigate this possibilty, in Fig. 12, we plot the total binding energy of two chemisorbed H atoms on their host cluster as function of the binding energy of only the H^+_{chem} atom of the corresponding $2H_{chem}$ pair. Corresponding data from references 21 and 22 are also included. We also include data calculated for C2/C1 adsorption of two H atoms on the $(MgO)_6$ cluster, the nano-olivine_b and nano-olivine_c clusters based on the initial C2-type H adsorptions shown in Fig. 5. The plot clearly shows a linear

relation between the two energies whereby the greater the binding energy of H^+_{chem}, the stronger the $2H_{chem}$ binding energy. This trend is clearly similar to the BEP relation in Fig. 10, suggesting that the H^+_{chem} binding energy is a good indicator of the relative TS[$2H_{chem} \rightarrow H_{2,phys}$] transition state barrier height. (this relation is further confirmed in a plot of the TS[$2H_{chem} \rightarrow H_{2,phys}$] transition state barrier height versus the H^+_{chem} binding energy – see Supplementary Information). The relatively extended data set in the plot of Fig. 12 allows us to analyse further the trends in H_2 dissociation/formation with respect to $2H_{chem}$ adsorption. In the inset to Fig. 12 we select ten data points from the main graph: five points corresponding to C1/C3 adsorption, and five points corresponding to C2/C1 adsorption. This selection of points highlights that for smaller H^+_{chem} binding energies the C1/C3 mode of $2H_{chem}$ adsorption yields a higher total binding energy, whereas for higher H^+_{chem} binding energies the C2/C1 mode tends to be energetically more favoured. The linear fits to the two sets of five points in the inset to Fig. 12 highlight these trends. In turn, these tendencies indicate that H_2 formation (i.e. smaller TS[$2H_{chem} \rightarrow H_{2,phys}$] transition state barriers) will tend to be via C1/C3 adsorbed H atoms, and H_2 dissociation will tend to proceed more via C2/C1 adsorbed H atom configurations. We further see from our results that strong C2/C1 adsorption can occur on relatively Mg-rich olivinic clusters with less compact structures, but seems not to be common on comparatively Mg-poor pyroxene clusters. Overall, we may speculate that amorphous/porous grains with forsteritic composition are more likely to dissociate H_2 molecules, and that less Mg-rich silicate grains (e.g. enstatite composition) or more crystalline/compact silicate grains in general are more likely to assist in the formation of H_2 from adsorbed H atoms.

Finally, we assess the thermal stability of the clusters taking into account the likely temperature increase due to exothermic H_2 formation. Here we assume that one H_2 molecule is formed at a time and that half of the released energy (-217 kJ/mol) goes into heating the dust and the remainder into exciting the degrees of freedom of the H_2 molecule. In order to calculated the temperature rise we use the heat capacity of the cluster in question which can estimated from a product of the contributions from each harmonic vibrational mode. The constant volume heat capacity, Cv was thus calculated from vibrational frequencies analysis for the nano-olivine_c and the nanopyroxene clusters, and found to be 71.6 cal mol^{-1} K^{-1} and 65.8 cal mol^{-1} K^{-1}, respectively. From these data we can calculate that H_2 formation leads an approximate increase of the temperatures of the nano-olivine_c and nanopyroxene clusters by 725 K and 789 K, respectively**.** Using a similar approach, Navarro-Ruiz et al.[8] estimated that H_2 formation on (010) forsterite surface would induce a bulk temperature increase of only 53 K. As our temperature increase for an ultrasmall silicate dust grain is significantly higher than that expected for a large bulk-like dust grain, we have explicitly studied the thermal stability of our clusters at 800 K for 25 ps using AIMD calculations. In the Supplementary Information we show various typical snapshots of the structures of the two clusters from these calculations. Although in each case the clusters are distorted from their 0 K optimised

structures the clusters do not break apart or melt. We note that the appearance of bond being broken or formed in the snapshots is largely due to arbitrary bond length cut-offs in the visualisation rather than any true chemical re-ordering. The closeness of the thermally distorted structures to their respective 0 K optimised structure was tested by taking a wide selection of snapshots and optimising their structures to the nearest local minimum. In nearly all cases the original 0 K structure, or an energy equivalent symmetry-transformed isomer, was found. Examples of structures leading to the latter can be seen at 22.11 ps for the nano_olivine_c clusters and at 24.47 ps for the nano_pyroxene cluster. In very few cases a slightly more symmetric, though slightly metastable isomer, was also found, having an overall structure which was very similar to the original non-symmetric structure. Snapshots at 10.39 ps for nano_olivine_c and at 12.23 ps for nano_pyroxene (see Fig. 14) show cluster structures that yielded these slightly metastable symmetric isomers. In addition, we made a quantitative estimate of the thermally induced structural disorder by calculating the relative root mean square interionic distance fluctuations employing a cluster-adapted Lindemann index (δ), see e.g., Ref. [35]. Typically one expects $\delta \geq 0.1$ for systems that are melted, or at least significantly thermally distorted. Although not a rigorous criterion, it is most likely that misleading large values of δ occur through pre-melting effects[36] rather than a small δ values incorrectly pointing to non-melting. In Fig. 14 we give the total Lindemann index (δ_{Total}) taking into account all atoms of the respective cluster and also the Lindemann index from only taking into account atom of the same type in a cluster ($\delta_{X,}$ where X=Si, O, Mg). Here we see both $\delta_{Total}<0.07$ and $\delta_X<0.07$ clearly confirming the non-melted character of each cluster and the relatively low degree of structural disorder at 800 K. In each case we also see that $\delta_{Si}<\delta_{Mg}$ and $\delta_{Si}<\delta_O$ showing that the Si atoms are the least perturbed atom type, in line with their 4-coordinated strong directional Si-O bonding which is never seen to be broken during the AIMD runs. The more isotropic ionic interactions between Mg and O ions allows for more structural distortion which allows for the small structural changes observed in each cluster. Following the analysis in ref 8, we expect the radiative dissipation of the heat released into small clusters by H_2 formation to be very rapid.

Conclusions

We have performed extensive DFT calculations to investigate the trends in H atom adsorption and H_2 formation and dissociation on nanoscale magnesium silicate clusters as a means to help understand H-based chemistry on silicate dust grains in the ISM. We consider small inherently non-crystalline clusters of both olivine and pyroxene composition and calculate H adsorption energies and barrier heights for the $2H_{chem} \rightarrow H_{2,phys}$ reaction. We find two $2H_{chem}$ types: (i) C1/C3 type which comes about through a $H^+_{chem} \rightarrow H^-_{chem}$ process, and (ii) C2/C1 type which results from a $H^-_{chem.} \rightarrow H^+_{chem}$ adsorption sequence. In both cases the resultant $2H_{chem}$ binding energies with the cluster are

found to be proportional to the corresponding $2H_{chem} \rightarrow H_{2,phys}$ transition state barrier for all cases considered confirming the generality of a BEP relation for such systems. Further, considering a related relation between the binding energy of only the H^{+}_{chem} with the bare cluster and the total binding energy of the two H atoms with the cluster, we suggest that there is a crossover between C1/C3 adsorption which promotes H_2 formation for smaller $2H_{chem}$ binding energies, and C2/C1 adsorption which favours H_2 dissociation for relatively higher $2H_{chem}$ binding energies. Based on where such types of adsorption modes have been found, we speculate that amorphous/porous grains with forsteritic composition are more likely to dissociate H_2, and that relatively Mg-poor silicate grains (e.g. enstatite composition) or more crystalline/compact silicate grains in general would tend to catalyse H_2 formation. By directly simulating the dynamics of two example nanosilicate clusters at 800 K, our ultrasmall grains are assessed to have high thermal structural stability with respect to the heat released during exothermic H_2 formation reactions.

Acknowledgments

S.T.B. acknowledges support from Spanish Government grants (Grant FIS2008-02238 and MAT2012-30924) and Generalitat de Catalunya grants (2014SGR97 and XRQTC). I.O. is thankful to the European Community FP7-ITN Marie Curie Programme (LASSIE project, Grant agreement no. 238258) and to (MERST, Tunisia) for a four month grant. The calculations were performed at the IDRIS and CINES French National Computer centers under projects 2012046838 and 2013046838. We also thank Fedor Goumans for allowing access to some initial structures for C1-type H_{chem} configurations on the nano-pyroxene cluster.

Table 1. Binding energies (kJ/mol) of physisorbed H atoms on the nano-pyroxene and nano-olivine_a clusters. Note that both our own data and cited literature data relate to calculated values that have not been corrected for BSSE effects and are thus typically overestimated by 3-6 kJ/mol (see main text, Supplementary Information and ref. 8). Values in brackets are in Kelvin.

Nano-cluster	Physisorption type	Previous Calculations	This work
Nano-pyroxene	**P2**	-	11 [1316], 19 [2312]
Nano-olivine_a	**P1**	[788], [1661]	7 [864] (Fig.2e)
	P2	[1327], [2063], [1240]	9 [1045] (Fig.2c), 16 [1876] (Fig.2d)
	P3	[1036-2894]	17 [1999] (Fig.2f), 5 [644]

[α] Kerkeni and Bromley[21]
[β] Navarro-Ruiz et al.[8]
[γ] Goumans et al. [22]

Table 2. Binding energies (kJ/mol) of single chemisorbed H atoms corresponding to the configurations shown in Fig. 3 for the nano-pyroxene cluster, and in Fig. 4 and Fig. 5 for the nano-olivine_a, nano-olivine_b and nano-olivine_c clusters, are listed in column 3. Column 5 shows the chemisorption energy of the second H atom (kJ/mol) for each configuration in column 4 with respect to the initial configurations listed in column 2 (following labelling in Figs. 3-5). The $2H_{chem}$ chemisorption type is listed in column 6. Column 7 lists the total $2H_{chem}$ binding energy (kJ/mol) with respect to the corresponding bare relaxed cluster.

Nano-cluster	Configuration of the first H_{chem}	E_{bind} of the first H_{chem}	Configuration of the second H_{chem}	E_{bind} of the second H_{chem}	$2H_{chem}$ chemisorption type	Binding Energy (E_{bind})
Nano-pyroxene	Fig. 3a	69	Fig. 6d	311	C1/C3	380
	Fig. 3b	91	Fig. 6e	311	C1/C3	403
	Fig. 3c	145	Fig. 6f	311	C1/C3	456
	Fig. 3d	162	Fig. 6a	304	C1/C3	466
	Fig. 3e	177	Fig. 6c	311	C1/C3	488
	Fig. 3f	196	Fig. 6g	312	C1/C3	508
	Fig. 3g	200	Fig. 6b	310	C1/C3	511
Nano-olivine_a	Fig. 4a	43	Fig. 7a	309	C1/C3	352
	Fig. 4b	92	Fig. 7g	334	C1/C3	426
	Fig. 4c	121	Fig. 7b	310	C1/C3	431
	Fig. 4d	146	Fig. 7f	324	C1/C3	470
	Fig. 4e	188	Fig. 7c	310	C1/C3	499
	Fig. 4f	208	Fig. 7e	311	C1/C3	519
	Fig. 4g	272	Fig. 7d	311	C1/C3	582
	Fig. 5d	91	Fig. 9b	533	C2/C1	625
	Fig. 5e	105	Fig. 9a	529	C2/C1	634
Nano-olivine_b	Fig. 4h	253	Fig. 7h	334	C1/C3	588
	Fig. 5c	38	Fig. 9c	555	C2/C1	593
Nano-olivine_c	Fig. 3, Ref. 21	180	Fig. 4c, Ref. 21	313	C1/C3	493
	Fig. 5a	-74	Fig. 9d	521	C2/C1	448

Table 3. Reaction barriers, recombination energies and desorption energies (kJ/mol) for $H_{2,g}$ release are given in columns 2, 3 and 4, respectively starting from configurations of two chemisorbed H atoms (following labelling of adsorbed $2H_{chem}$ configurations in Figs. 6, 7 and 9).

Initial configuration	$2H_{chem} \rightarrow H_{2,phys}$	TS [$2H_{chem} \rightarrow H_{2,phys}$]	$H_{2,phys} \rightarrow H_{2,g}$
Fig. 6a	2	55	9
Fig. 6b	37	102	20
Fig. 6c	14	-	20
Fig. 6d	-94	8	20
Fig. 6e	-71	45	20
Fig. 6f	-18	74	20
Fig. 6g	21	-	33
Fig. 7a	-123	-	20
Fig. 7b	-43	34	20
Fig. 7c	24	90	20
Fig. 7d	114	137	14
Fig. 7e	41	72	24
Fig. 7f	-3	51	20
Fig. 7g	-44	22	16
Fig. 9a	159	188	12
Fig. 9b	163	195	17

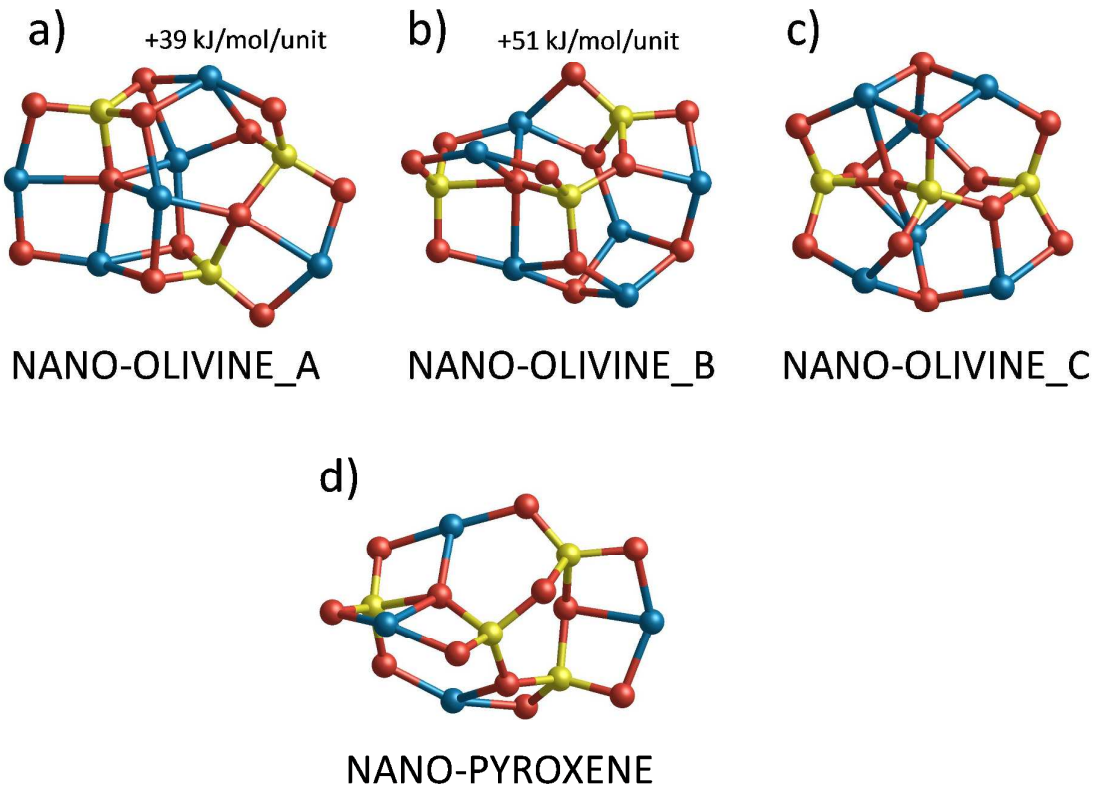

Fig. 1. Optimized structures of: a) nano-olivine_a, b), nano-olivine_b, c) and nano-olivine_c cluster isomers (all with composition $(MgO)_6(SiO_2)_3$,), and d) the nano-pyroxene cluster (composition $(MgO)_4(SiO_2)_4$). The nano-olivine relative energies are per $(MgO)_2(SiO_2)$ formula unit with respect to the nano-olivine_c ground state. Atom key: Si - yellow, Mg - blue and O - red.

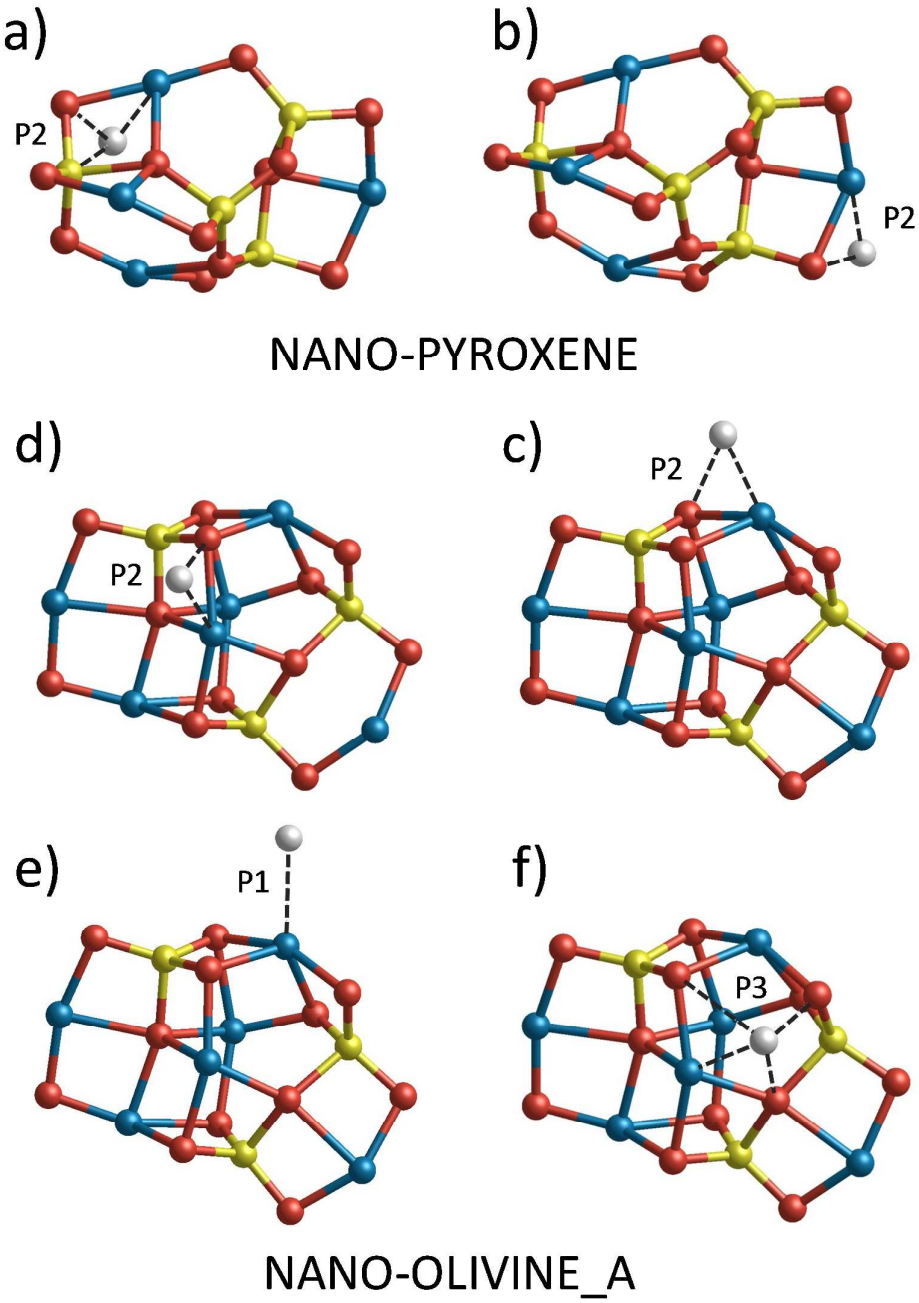

Fig. 2. Physisorption sites (P1, P2 and P3) for a single physisorbed H atom on the $(MgO)_4(SiO_2)_4$ nano-pyroxene cluster (a, b), and on the $(MgO)_6(SiO_2)_3$ nano-olivine_a cluster (c-f). Grey dashed lines highlight all interatomic distances between the H atom and the respective cluster that are ≤2.7Å. Atom key: Si - yellow, Mg - blue and O - red.

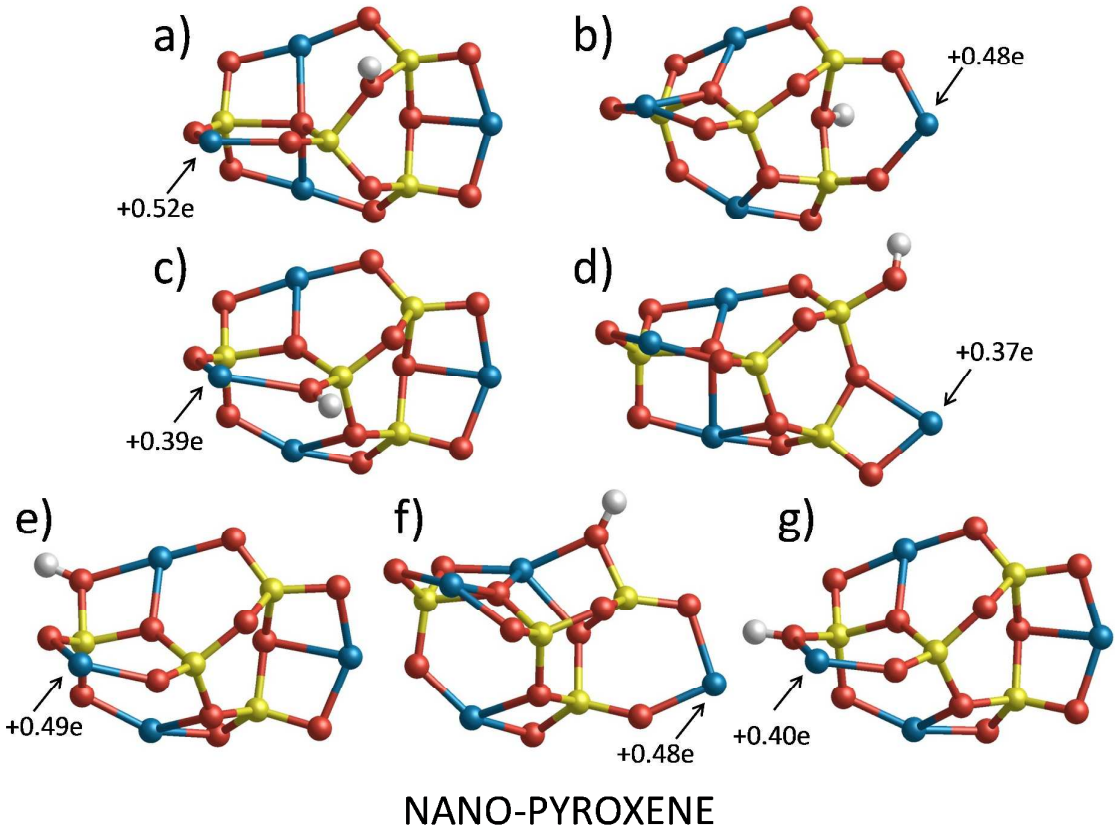

Fig. 3. C1-type H chemisorption configurations on the on the $(MgO)_4(SiO_2)_4$ nanopyroxene cluster ordered by increasing E_{bind} values (a-g). The Mg atom that receives the negative charge in each case is indicated by an arrow and the corresponding negative charge increase. Atom key: Si - yellow, Mg - blue and O - red.

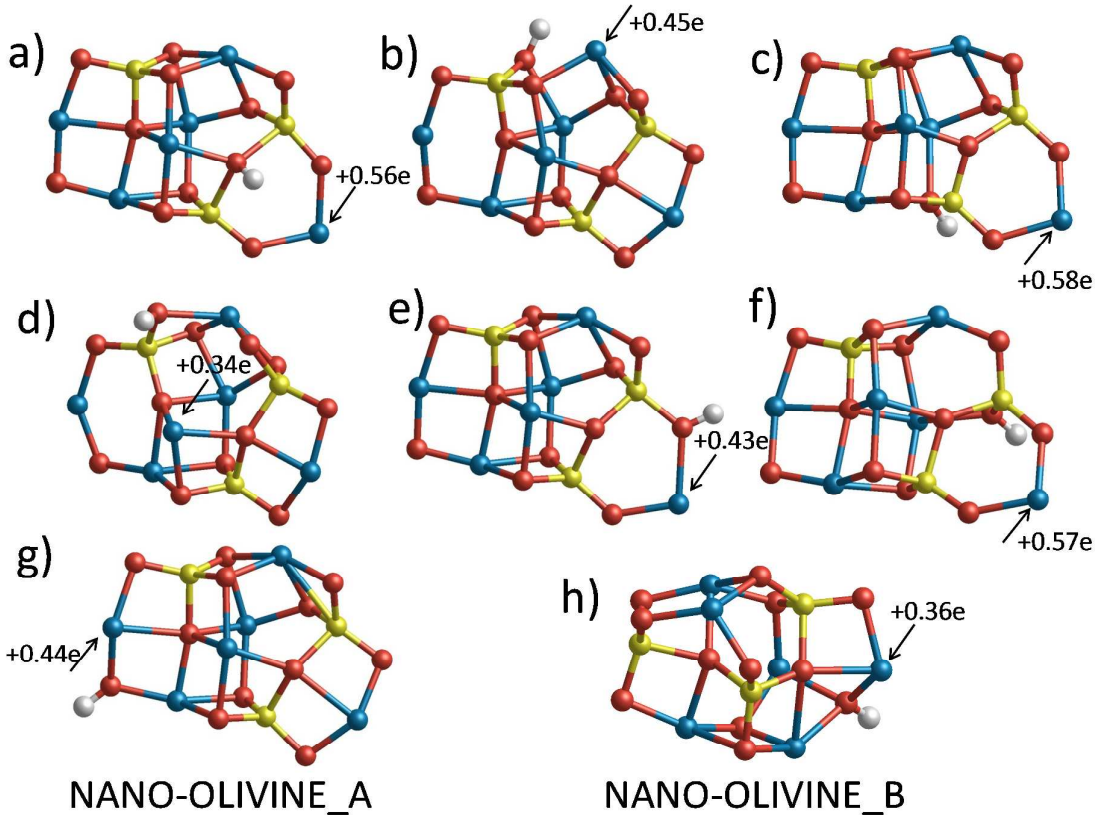

Fig. 4. C1-type H chemisorption configurations on the $(MgO)_6(SiO_2)_3$ nano-olivine_a cluster a)-g), ordered by increasing E_{bind} values, and on the $(MgO)_6(SiO_2)_3$ nano-olivine_b cluster h). The Mg atom that receives the negative charge in each case is indicated by an arrow and the corresponding negative charge increase. Atom key: Si - yellow, Mg - blue and O - red.

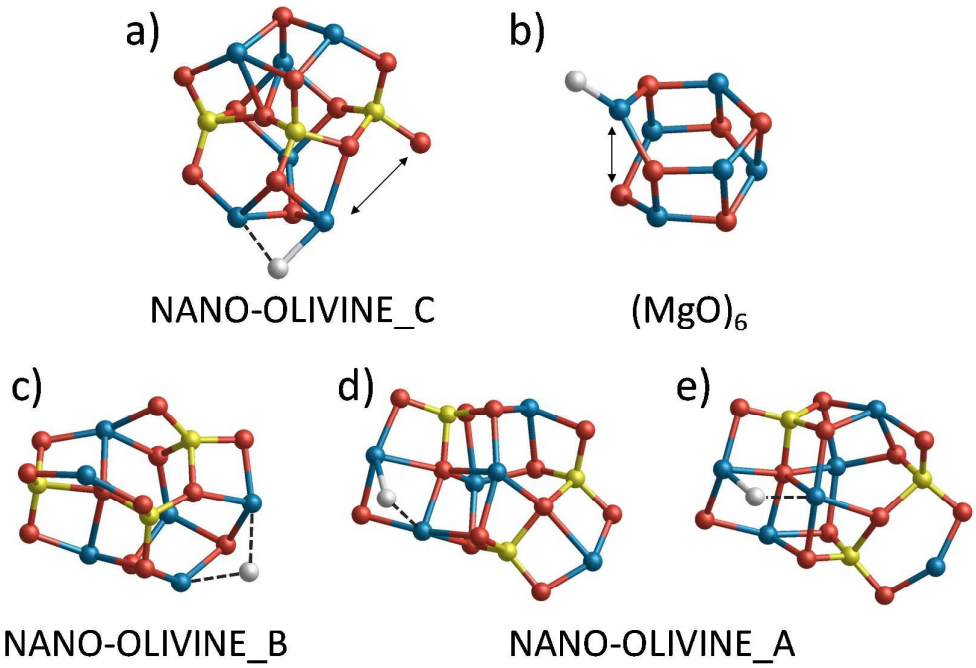

Fig. 5. C2-type H chemisorption configurations on: a), the $(MgO)_6(SiO_2)_3$ nano-olivine_a cluster, b) a $(MgO)_6$ cluster, and c-e) the $(MgO)_6(SiO_2)_3$ nano-olivine_a clusters. Grey dashed lines highlight all interatomic distances between the H atom and the respective cluster which are >1.9 Å and ≤2.7 Å. H-Mg distances which are ≤1.9 Å are drawn as bonds. Double headed arrows indicate Mg-O bond breakage induced upon H adsorption. Atom key: Si - yellow, Mg - blue and O - red.

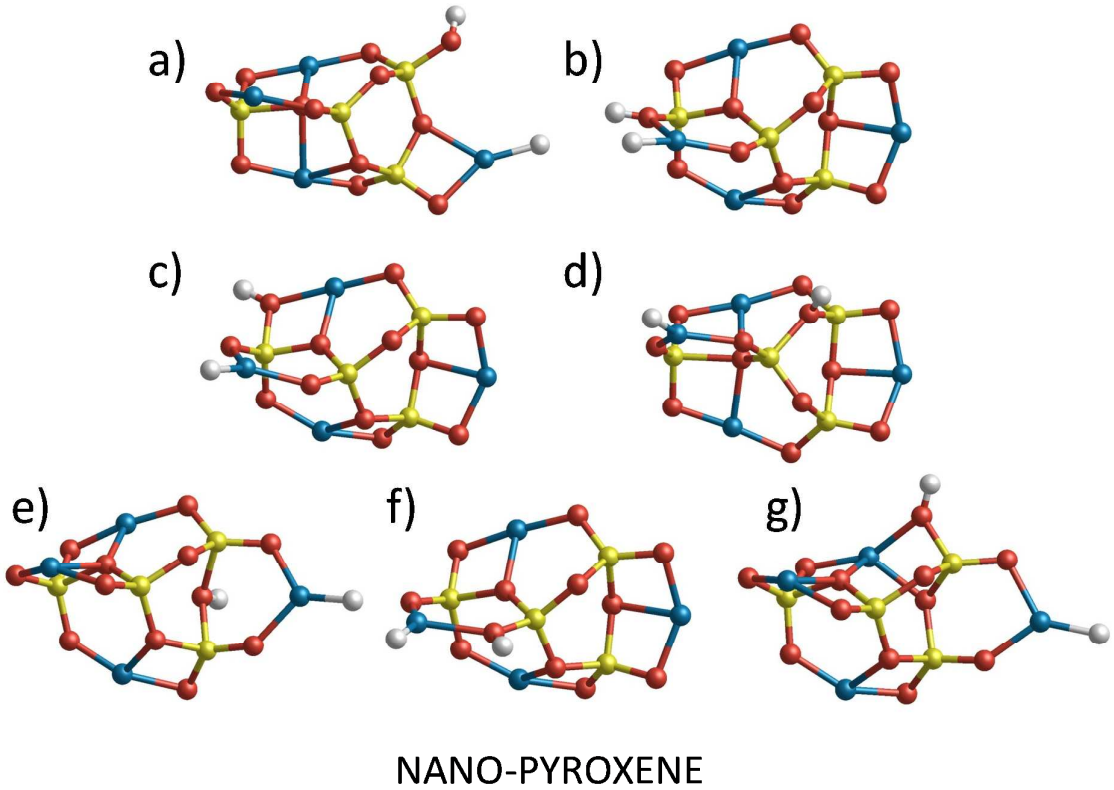

Fig. 6. C1/C3-type $2H_{chem}$ configurations on the $(MgO)_6(SiO_2)_3$ nano-olivine_a cluster ordered by increasing E_{bind} of H atom which is bound to a Mg atom relative to the correspoonding cluster with one chemisorbed H atom on a C1 site. Atom key: Si - yellow, Mg - blue and O - red.

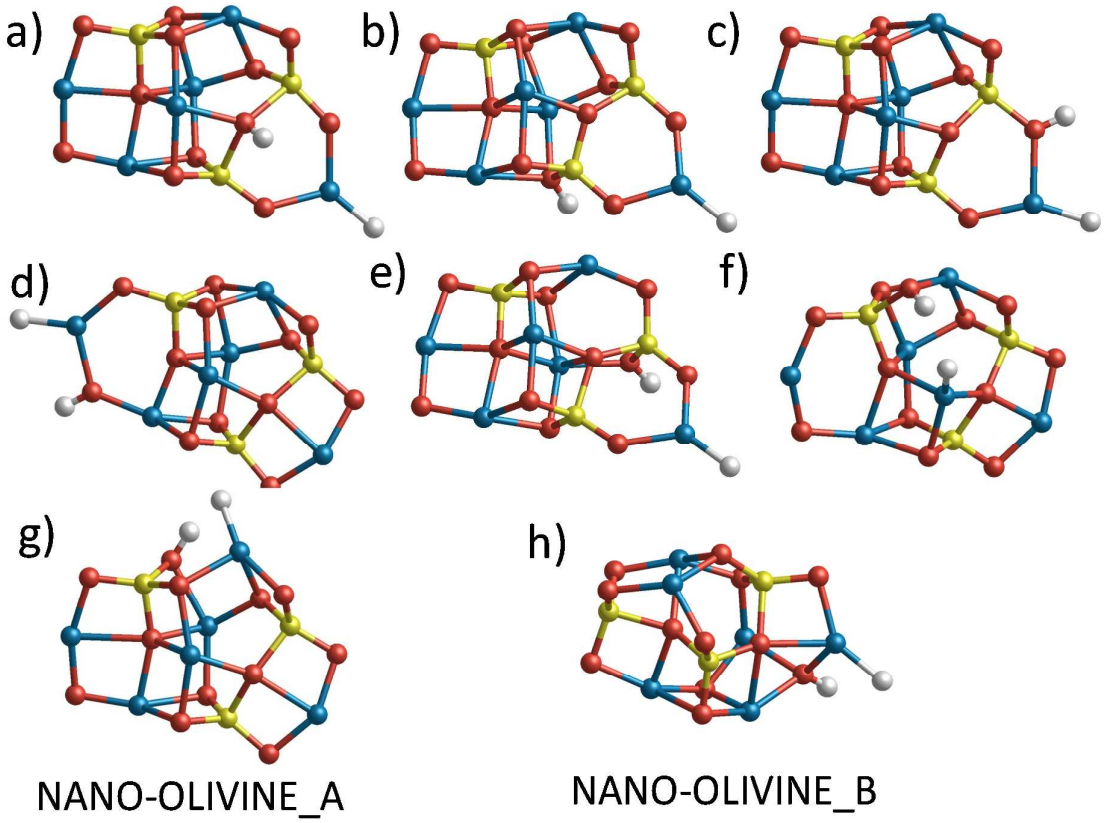

Fig. 7. C1/C3-type $2H_{chem}$ configurations on the $(MgO)_4(SiO_2)_4$ nanopyroxene cluster ordered by increasing E_{bind} of the H atom which is bound to a Mg atom relative to the corresponding cluster with one chemisorbed H atom on a C1 site. Atom key: Si - yellow, Mg - blue and O - red.

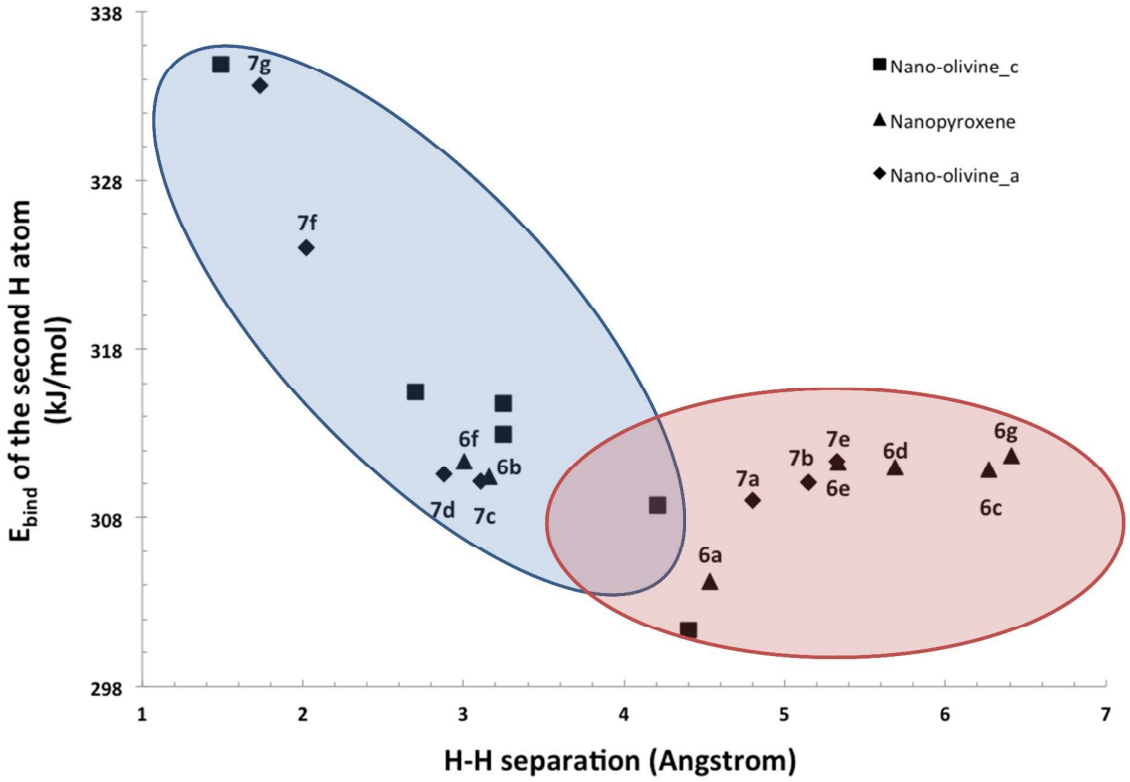

Fig. 8. Plot of binding energy of the second chemisorbed H^-_{chem} atom on the nano-olivine_a and nano-pyroxene clusters versus H-H separation for C1/C3 type $2H_{chem}$ adsorption (i.e. $[H^+_{chem} \rightarrow H^-_{chem}]$) Labelling corresponds to the configurations in Fig. 6 for the nano-pyroxene cluster and in Fig.7 for the nano-olivine_a cluster. Data from Kerkeni and Bromley[21] corresponding to the nano-olivine_c cluster is also included. The blue shaded area roughly encircles data points for which the corresponding $H^+_{chem.}$+H^-_{chem} pairs are electrostatically stabilised. The red shaded area roughly encircles data points for which the corresponding $H^+_{chem.}$+H^-_{chem} pairs appear not to be significantly affected by electrostatics.

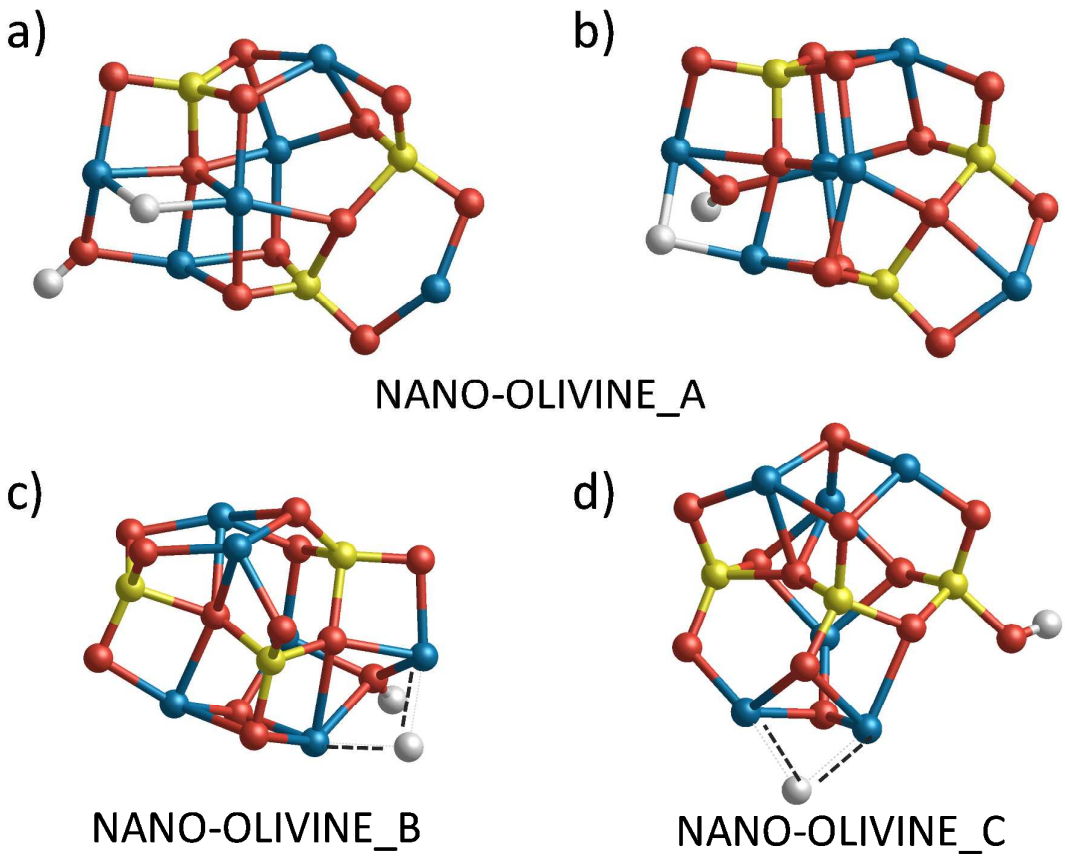

Fig. 9. C1/C2-type $2H_{chem}$ configurations on: a-b) the nano-olivine_a cluster, c) the nano-olivine_b cluster and d) the nano-olivine_c cluster, all with $(MgO)_6(SiO_2)_3$ composition. Atom key: Si - yellow, Mg - blue and O - red.

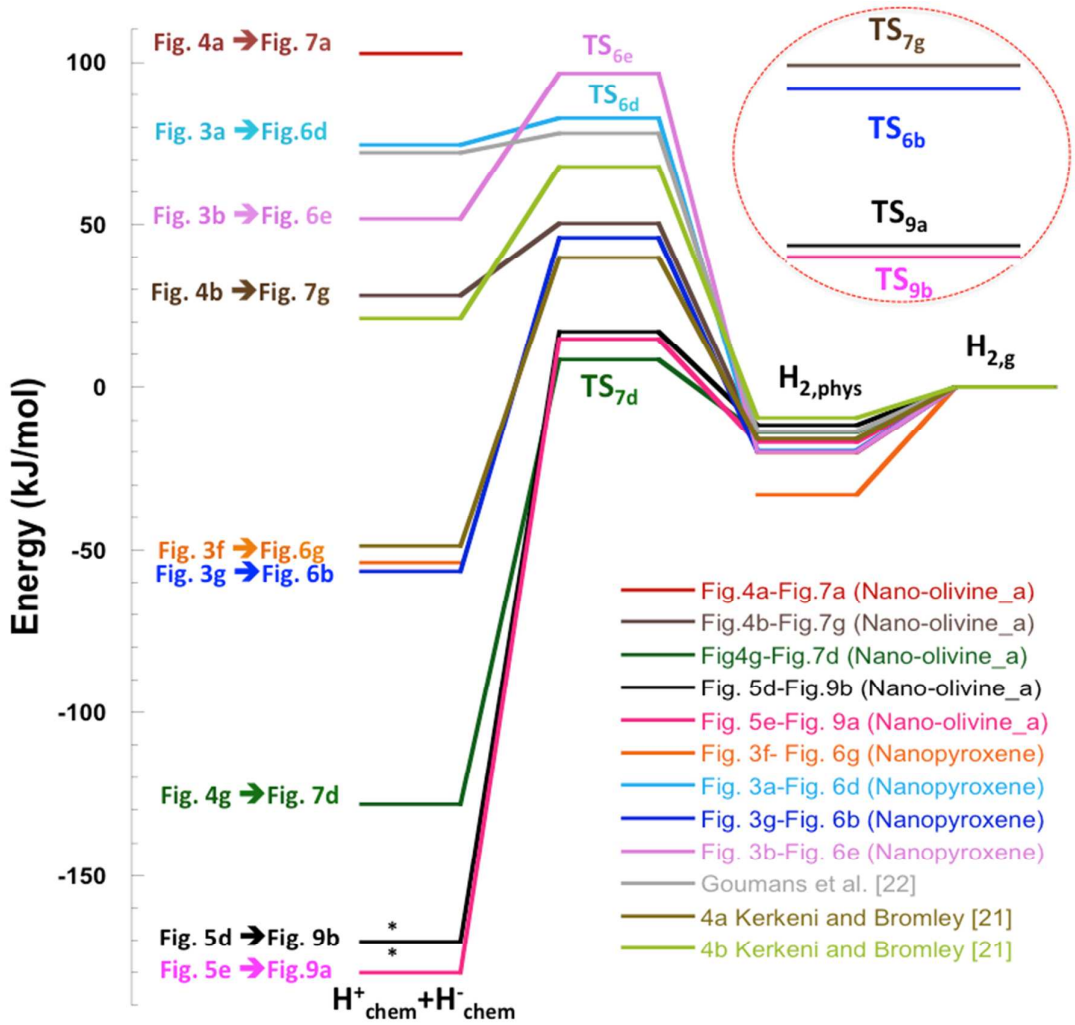

Fig. 10. A selection of pathways for the $2H_{chem} \rightarrow H_{2,g}$ reaction on the nano-olivine_a cluster and on the nano-pyroxene cluster. The y-axis refers to energies relative to the sum of the energies of the bare relaxed nano-olivine_c cluster and a $H_{2,g}$ molecule (see also ref 21). The pathway labelling refers to the structures in the corresponding figures and denote the manner in which the initial state $2H_{chem}$ was found. For example the pathway label "Fig. 5e → Fig. 9a" signifies that the starting $2H_{chem}$ configuration is that of Fig. 9a, which was derived from adding a H atom to the structure found in Fig. 5e. The two "*"s correspond to pathways starting from C2/C1 type $2H_{chem}$ adsorption. The "TS" labels refer to transition states for the $2H_{chem} \rightarrow H_{2,phys}$ reaction found in this study, where the subscripts relate to the figure showing the corresponding initial $2H_{chem}$ configuration (all TS structures can be found in the Supplementary Information). The inset encircled by a dashed line is a magnified portion of the main plot showing transition state labels. Data for corresponding reaction pathways on the foresterite (010) surface (ref. 22), and on the nano-silicate_c cluster (ref. 21) are also included.

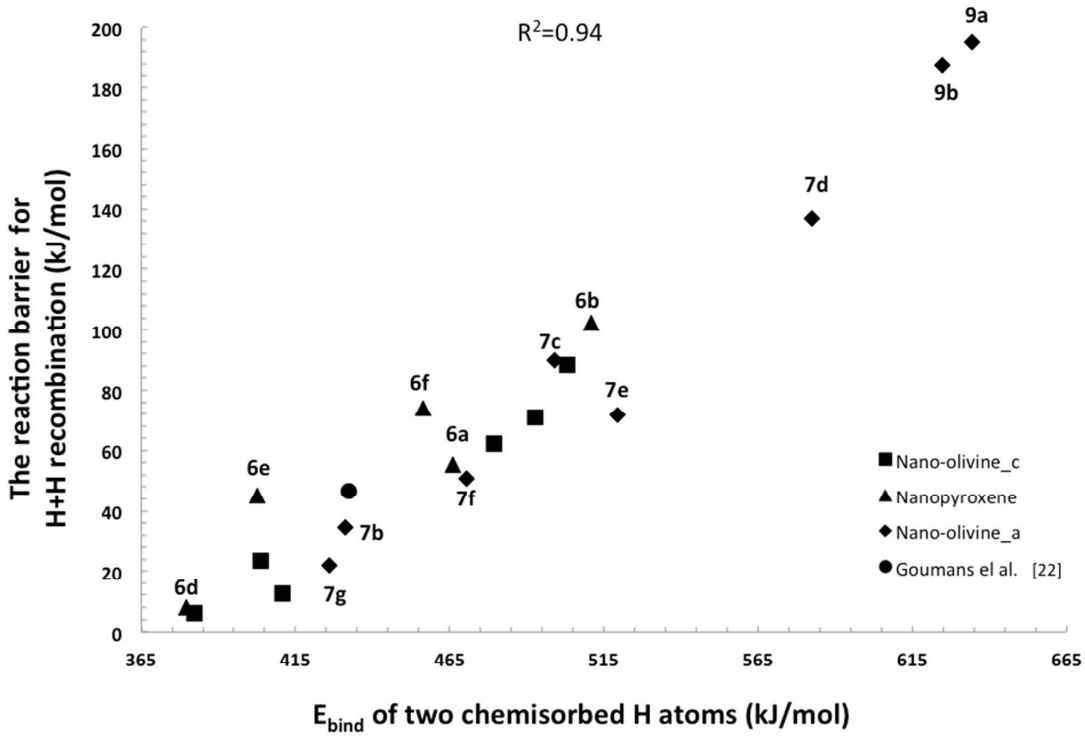

Fig. 11. $2H_{chem} \rightarrow H_2$ recombination barrier height versus the total binding energy of two chemisorbed H atoms for all considered reaction paths on the nano-olivine_a and nano-pyroxene clusters. The labelling of the data points follows that in Figs. 6, 7 and 9. Data from Goumans *et al.*[22] corresponding to the foresterite (010) surface and from Kerkeni and Bromley[21] corresponding to the nano-olivine_c cluster are also shown. The high coefficient of determination (R^2) confirms the strong linearity of the relation (fitting line not shown).

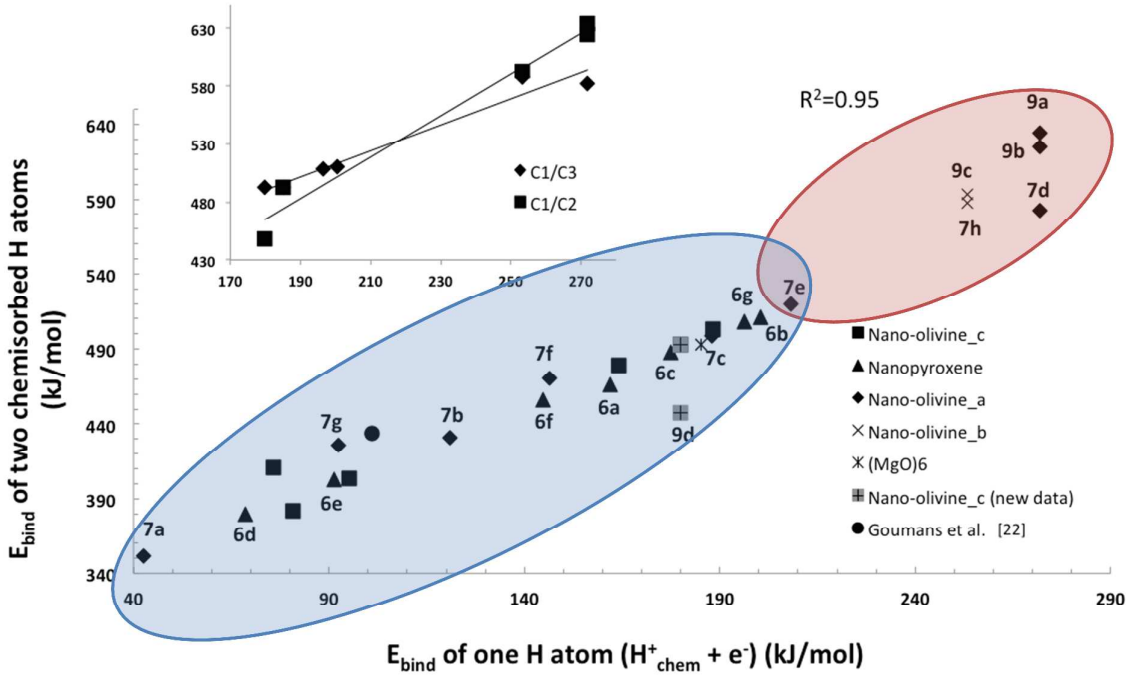

Fig. 12. The total binding energy versus binding energy of one H atom chemisorbed to the respective bare cluster in a C1 mode (i.e. H^{+}_{chem}) for all considered nano-olivine and nano-pyroxene clusters and the $(MgO)_6$ cluster in Fig. 5. The labelling of the data points for the nanosilicates follows that in Figs. 6, 7 and 9. Data from Goumans et al.[22] corresponding to the foresterite (010) surface and from Kerkeni and Bromley[21]corresponding to the nano-olivine_c cluster are also shown (new data for nano-olivine_c from this study is labelled). Red shading highlights data points with both high $2H_{chem}$ and high H^{+}_{chem} binding energies, all of which correspond to nano-olivine clusters, and most of which to metastable nano-olivine isomers. The blue shading highlights trend of the remaining data points which correspond to a mix of nano-olivine and nano-pyroxene clusters. The high coefficient of determination (R^2) confirms the strong linearity of the relation for all data points in the main plot (fitting line not shown). The inset highlights the separate trends in the strength of C1/C2 *versus* C1/C3 types of 2H chemisorption with respect to binding energy of the C1-bound H_{chem} atom. The fitting lines indicate a crossover in energetic favourability from C1/C3 type chemisorption to C1/C2 chemisorption with increasing chemisorption strength of the C1-bound H_{chem} atom.

References

[1] E. Herbst, *Chem. Soc. Rev*., 2001, 30, 168-176.

[2] D. Hollenbach and E. E. Salpeter, *Astrophys. J.*, 1971, 163,155-160.

[3] W. W. Duley and D. A. Williams, 1984, Interstellar chemistry, Academic Press, New York.

[4] D. A. Williams, 2003, in V. Pirronello, J. Krelowski, G. Manico, eds Solid state astrochemistry, Kluwer, Dordrecht, 1.

[5] J. L. Lemaire, G. Vidali, S. Baouche, M. Chehrouni, H. Chaabouni and H. Mokrane, *Astrophys. J.*, 2010, 725, L156-160.

[6] F. Islam, C. Cecchi-Pestellini, S. Viti and S. Casu, *Astrophys. J.*, 2010, 725, L1111 – 1123.

[7] J. Le Bourlot, F. Le Petit, C. Pinto, E. Roueff and F. Roy, 2012, Astronom. Astrophys., 541, A76-94.

[8] J. Navarro-Ruiz, M. Sodupe, P. Ugliengo and A. Rimola, *Phys. Chem. Chem. Phys.*, 2014, **16**, 17447-17457.

[9] A. S. Ferrarotti, H. –P. Gail, Astronom. Astrophys., 2006, 447, 553-576.

[10] I. Cherchneff, Astronom. Astrophys., 2006,456, 1001-1012.

[11] S. T. Bromley, T. P. M. Goumans, E. Herbst, A.P. Jones, B. Slater, *Phys. Chem. Chem. Phys*, 2014, 16, 18623-18643.

[12] T. P. M. Goumans and Stefan T. Bromley, *Mon. Not. R. Astron. Soc.*, 2011, 414, 1285-1291.

[13] A. Li and B. T. Draine, *Astrophys. J.*, 2001, 550, L213-L217.

[14] V. Pirronello, C. Liu, L. Shem and G. Vidali, *Astrophys. J.*, 1997, 475, L69-L72.

[15] H. B. Perets, A. Lederhendler, O. Biham, G. Vidali, L. Li, S. Swords, E. Congiu, J. Roser, G. Manicó, J. R. Brucato and V. Pirronello, *Astrophys. J.*, 2007, 661, L163-L166.

[16] G. Vidali, V. Pirronello, L. Li, J. Roser, G. Manicó, E. Congiu, H. Mehl, A. Lederhendler, H. B. Perets, J. R. Brucato and O. Biham, *J. Phys. Chem. A.*, 2007, 111, 12611- 12619.

[17] L. Gavilan, J. L. Lemaire and G. Vidali, *Mon. Not. R. Aston. Soc.*, 2012, 424, 2961-2970.

[18] S. T. Bromley, T. P. M. Goumans, E. Herbst, A. P. Jones and B. Slater, *Phys. Chem. Chem. Phys.*, 2014,16, 18623-18643

[19] T. P. M. Goumans and S. T. Bromley, *Mon. Not. R. Astron. Soc.*, 2012, 420, 3344-3349.

[20] T. P. M. Goumans and S. T. Bromley, *Phil. Trans. R. Soc. A*, 2013, 371, 20110580.

[21] B. Kerkeni and S.T. Bromley, *Mon. Not. R. Astron. Soc.*, 2013, 435, 1486-1493.

[22] T. P. M. Goumans, C. Richard A. Catlow and Wendy A. Brown, *Mon. Not. R. Astron. Soc.*, 2009, 393, 1403-1407.

[23] S. Garcia-Gil, D. Teillet-Billy, N. Rougeau, and V. Sidis, *J. Phys. Chem. C*., 2013, 117, 12612−12621

[24] C. A. Downing, B. Ahmady, C. R. A. Catlow and N. H. de Leeuw, *Phil. Trans. R. Soc. A.*, 2013, 371, 20110592.

[25] M. J. Frish et al., 2004, Gaussian 09, Revision A.02. Gaussian Inc., Walling-ford, CT, 2009.

[26] Y. Zhao and D.G. Truhlar, *J. Phys. Chem. A.*, 2004, 108, 6908-6918.

[27] Y. Zhao and D.G. Truhlar, *J. Phys. Chem. A.*, 2005, 109, 5656-5667.

[28] T. P. M. Goumans, C. Richard A. Catlow, W. A. Brown, J. Kastner and P. Sherwood, *Phys. Chem. Chem. Phys.*, 2009, 11, 5431-5436.

[29] H. B. Schlegel, J. Comp. Chem., 1982, 3, 214-218.

[30] G. Bussi, D. Donadio and M. Parrinello, J. Chem. Phys. 2007, 126, 014101(1-7)

[31] J. P. Perdew, K. Burke, and M. Ernzerhof, Phys. Rev. Lett., 1996, 77, 3865-3868.

[32] V. Blum, R. Gehrke, F. Hanke, P. Havu, V. Havu, X. Ren, K. Reuter, and M. Scheffler, Comp. Phys. Commun., 2009, 180, 2175-2196.

[33] N. Katz, I. Furman, O. Biham, V. Pirronello and G. Vidali, Astrophys. J., 1999, 522, 305-12

[34] J. Arsic, D. Kaminski, M. Radenovic, P. Poodt, W. S. Graswinckel, H. M. Cuppen and E. Vlieg, J. Chem. Phys., 2004, 120, 9720-9724

[35] J. Jellinek, T. L. Beck and R. S. Berry, J. Chem. Phys.,1986, 84, 2783-2794.

[36] F. Viñes, J. Carrasco, and S. T. Bromley, Phys. Rev. B, 2012, 85, 195425(1-6).